

Constraints on the γ -parameter for the vacuum solution of Cotton gravity with geodesics and shadows

Ednaldo L. B. Junior,^{1,*} José Tarciso S. S. Junior,^{2,†} Francisco S. N. Lobo,^{3,4,‡}
Manuel E. Rodrigues,^{2,5,§} Diego Rubiera-Garcia,^{6,¶} Luís F. Dias da Silva,^{3,**} and Henrique A. Vieira^{2,††}

¹*Faculdade de Física, Universidade Federal do Pará,
Campus Universitário de Tucuruí, CEP: 68464-000, Tucuruí, Pará, Brazil*

²*Faculdade de Física, Programa de Pós-Graduação em Física,
Universidade Federal do Pará, 66075-110, Belém, Pará, Brazil*

³*Instituto de Astrofísica e Ciências do Espaço, Faculdade de Ciências da Universidade de Lisboa,
Edifício C8, Campo Grande, P-1749-016 Lisbon, Portugal*

⁴*Departamento de Física, Faculdade de Ciências da Universidade de Lisboa,
Edifício C8, Campo Grande, P-1749-016 Lisbon, Portugal*

⁵*Faculdade de Ciências Exatas e Tecnologia, Universidade Federal do Pará,
Campus Universitário de Abaetetuba, 68440-000, Abaetetuba, Pará, Brazil*

⁶*Departamento de Física Teórica and IPARCOS,
Universidad Complutense de Madrid, E-28040 Madrid, Spain*

(Dated: August 1, 2024)

We consider a recently introduced extension of General Relativity dubbed as Cotton gravity (CG), based on the use of the Cotton tensor, to estimate the size of a new constant γ appearing within a spherically symmetric, vacuum solution of the theory. Taking into account its non-asymptotically flat character, we use the inferred size of the central brightness depression of the supermassive object at the heart of the Milky Way galaxy (Sgr A*) by the Event Horizon Telescope to constrain at 2σ the CG parameter as $\gamma M \approx 3.5 \times 10^{-12}$. We study the potential observational consequences from the smallness of such a value using exact and numerical expressions for the deflection angle, optical images from optically and geometrically thin accretion disks, isoradials, and instability scales (Lyapunov index) of nearly bound geodesics associated to photon rings. Our results point towards the impossibility to distinguish between these two geometries using current and foreseeable techniques in the field of interferometric detection of optical sources.

I. INTRODUCTION

Despite the undeniable success of Einstein's General Relativity (GR) in explaining a large number of gravitational phenomena in different regimes [1], there are several drawbacks of the theory. On the one hand, the accelerated expansion of the Universe, as found by Type-Ia supernovae observations [2, 3], can only be accounted for, in the frame of GR, via a hypothetical fluid known as dark energy [4], whose properties can be assimilated to that of a cosmological constant term [5] yet there is no direct proof of its existence. Similarly, the explanation of galactic rotation curves demands more than 90% of the total mass of most galaxies to be dominated by a non-baryonic form of matter dubbed as dark matter [7], which we have been unable to detect in any terrestrial observatory yet. On more theoretical grounds, the problems with the unavoidable development of space-time singularities inside black holes and in the early cosmological evolution and the loss of predictability they bring about

[6], the Hawking process and the associated information loss paradox [8], and the development of a framework unifying gravity and quantum mechanics (quantum gravity [9]), are challenges that still haunt the gravitational community.

In response to these challenges, a large avenue of research has emerged in the last few decades arranged around alternative approaches to GR, generally dubbed as modified theories of gravity (see e.g. [10, 11] for some reviews). Within this context, recently Harada presented a theory called “Cotton Gravity” (CG) [12]. In this proposal, the effects describing gravity are attributed to the Cotton tensor, and the corresponding field equations contain third-order derivatives. The main interest in this proposal comes from the fact that any solution of the Einstein equations, with or without a cosmological constant term, also satisfies the field equations of CG. Furthermore, the cosmological constant itself emerges as an integration constant out of the field equations. In addition, in [13] Harada used the post-Newtonian limit of CG to solve the field equations numerically, interpreting the rotation curves of several galaxies without employing dark matter sources. Note that the possibility that dark matter may be geometric effects of modified theories of gravity has been explored in the literature [14–19].

Regarding new solutions within CG, the first non-trivial one with static, spherical symmetry was found in [13], which extends the Schwarzschild solution via a new

* ednaldobarrosjr@gmail.com

† tarcisojunior17@gmail.com

‡ fslobo@ciencias.ulisboa.pt

§ esialg@gmail.com

¶ drubiera@ucm.es

** fc53497@alunos.fc.ul.pt

†† henriquefisica2017@gmail.com

parameter γ . Other non-trivial solutions were found in [20, 21]. On the other hand, in [22] it was emphasized that the Codazzi tensor can be derived from the equations of CG, which implies that Harada’s formulation can be understood as a modification of the GR equations due to the presence of this residual tensor. This way, with the introduction of the Codazzi tensor, it became possible to express CG through a new formulation, which allowed for the representation of conformally flat cosmological solutions without a vacuum in CG [23]. However, there is ongoing debate about the viability of CG as a potential extension of GR. Some researchers see CG as promising for addressing GR’s limitations, while others doubt its theoretical consistency [24–27]. Further research is needed to determine whether CG can replace or complement GR, or if it will remain a theoretical curiosity.

In order to set constraints in the new parameter γ of CG, one can resort to the gravitational lensing of light. This is the deflection of light trajectories as they pass close to massive bodies (stars, black holes, galaxies, etc) and can act like a natural telescope by amplifying the source brightness and even creating multiple images. Recent developments related to this effect can be divided into two groups: microlensing (i.e. the measurement of the collective magnification of various images) and strong lensing [28]. For the sake of this work we are (mostly) interested in the strong field regime, given the fact that it offers the possibility of testing GR beyond the weak-field limit tests carried out so far. In such a limit, Bozza [29] proposed a formalism to calculate the deflection angle for every spherically symmetric metric in terms of a logarithmic expansion. Such a formalism has been very influential in advancing analytical methods to compare theoretical predictions with real images [30, 31], including alternative spherically symmetric metrics [32–35].

The black hole shadow and photon ring heuristics are two such examples of visual phenomena caused by strong gravitational lensing [36]. The former consists in the dark silhouette of a black hole that is projected in the celestial plane, with a critical boundary separating backwards-traced geodesics that are scattered towards infinity from those that are captured by a black hole [37, 38]. The latter appears as an infinite series of discrete and stacked, exponentially-damped in luminosity, lensed images of the emission surrounding a black hole, under the assumption of an optically thin and non-spherical accretion disk [39, 40]. The recent progress in high-frequency very-long-baseline interferometry (VLBI) provides a direct way of comparing such heuristics with actual images, by the Event Horizon Telescope (EHT) Collaboration, of the super-heated overflow of the plasma around the super-massive central objects of M87* [41] and Sgr A* [42]. In turn, this provides an unprecedented opportunity to perform tests of new gravitational Physics, which has been put to good use very recently, see e.g. [43].

The main aim of this work is therefore to make use of this opportunity to study the optical appearances of the CG black hole above. In particular, we shall employ the

reported bounds on Sgr A*’s shadow by the EHT Collaboration to constrain the CG black hole’s parameter space. Next, we generate images of this geometry within this restricted parameter space when illuminated by an optically and geometrically thin accretion disk, modeled by three semi-analytic emission profiles developed by Gralla-Lupsasca-Marrone (GLM) [44], and compare its optical appearance with that of a Schwarzschild black hole. Furthermore, we study the Lyapunov exponents of nearly bound orbits to elaborate on the differences between both geometries. In this work we consider units $G = c = 1$.

This paper is outlined in the following manner: In Sec. II, we briefly present the field equations of CG and the static, spherically symmetric metric used throughout this work. In Sec. III, we obtain the null geodesic equation and the effective potential of the CG black hole, using the above-mentioned spherically symmetric metric. Section IV addresses gravitational lensing in CG, where we first derive the exact analytical expression for the deflection angle using elliptic integrals, followed by an approximate expression for the weak field regime. In Sec. V, we generate the images of the Cotton black hole using the restricted γ -space parameter obtained in the previous sections, and qualitatively compare its appearance to that of a Schwarzschild black hole of the same mass parameter. In Sec. VI, we perform an analysis of isoradial curves in the Cotton and Schwarzschild space-times, to complement the black hole images presented in the previous section. In Sec. VII, we explore the Lyapunov exponent of nearly bound orbits, which is a quantity that measures the instability scale of these orbits. Finally, in Sec. VIII, we summarize our results and conclude.

II. A SPHERICALLY SYMMETRIC SOLUTION OF COTTON GRAVITY

Recently, as mentioned above, a generalization of the gravitational field equations of GR, dubbed as “Cotton Gravity” (CG) [12], was proposed. The field equations read as follows

$$C_{\alpha\mu\nu} = \kappa^2 \nabla_\beta \Theta^\beta_{\alpha\mu\nu}, \quad (1)$$

where $\kappa^2 = 8\pi$, is Newton’s constant in suitable units, ∇_β is the usual covariant derivative built with the Christoffel symbols of the metric, $C_{\alpha\mu\nu}$ is the Cotton tensor defined as

$$C_{\alpha\mu\nu} \equiv \nabla_\mu R_{\nu\alpha} - \nabla_\nu R_{\alpha\mu} - \frac{1}{6} (g_{\alpha\nu} \partial_\mu - g_{\alpha\mu} \partial_\nu) R, \quad (2)$$

where $R_{\mu\nu}$ stands for the Ricci tensor and R is the Ricci scalar, and finally the energy-momentum tensor $\Theta_{\beta\alpha\mu\nu}$ is defined as

$$\begin{aligned} \Theta_{\beta\alpha\mu\nu} \equiv & \frac{1}{2} (g_{\beta\mu} \Theta_{\alpha\nu} - g_{\alpha\mu} \Theta_{\beta\nu} - g_{\beta\nu} \Theta_{\alpha\mu} + g_{\alpha\nu} \Theta_{\beta\mu}) \\ & - \frac{1}{6} (g_{\beta\mu} g_{\alpha\nu} - g_{\alpha\mu} g_{\beta\nu}) \Theta, \end{aligned} \quad (3)$$

with $\Theta_{\beta\mu} = g^{\alpha\nu}\Theta_{\beta\alpha\mu\nu}$ and $\Theta = g^{\beta\mu}\Theta_{\beta\mu}$.

The most remarkable feature of CG gravity is that every solution of the Einstein equations with a cosmological constant term $G_{\mu\nu} + \Lambda g_{\mu\nu} = \kappa^2\Theta_{\mu\nu}$ satisfies Eq. (1) [12], while the opposite is not true. In contrast to GR, however, the cosmological constant in CG is determined by integration of the field equations. Furthermore, the conservation law ($\nabla_\beta\Theta^\beta{}_\nu = 0$) is a natural consequence of the theory, just like in GR, as can be verified by contracting Eq. (1) by $g^{\alpha\nu}$ to yield

$$g^{\alpha\nu}C_{\alpha\mu\nu} = \kappa^2\nabla_\beta\Theta^\beta{}_\nu = 0. \quad (4)$$

For the sake of this work we use the exact vacuum solution obtained by Harada in [13]. Similarly to GR, where $R_{\mu\nu} = 0$, this solution is obtained in Cotton Gravity when $C_{\alpha\mu\nu} = 0$ is considered. Such a solution belongs to the static, spherically symmetric class of metrics with line element

$$ds^2 = -A(r)dt^2 + \frac{dr^2}{A(r)} + C(r)(d\theta^2 + \sin^2\theta d\phi^2). \quad (5)$$

whose metric function reads as [12]

$$A(r) = 1 - \frac{2M}{r} - \frac{\Lambda}{3}r^2 + \gamma r, \quad C(r) = r^2. \quad (6)$$

This is the first non-trivial solution found in CG theory, which contains a new parameter γ , not present in the Schwarzschild case of the GR, and which breaks the asymptotically flat character of the space-time. Moreover, the cosmological constant is obtained naturally as an integration constant no matter the value of the cosmological constant Λ , which we take to be vanishing in this work. We draw attention to the fact that solutions containing a linear γr term have been obtained in other theoretical contexts (e.g. [45–49]).

III. GEODESICS AND EFFECTIVE POTENTIAL

A. Gravitational lensing

In this section, we obtain the null geodesic equation and the effective potential of the CG black hole, using the spherically symmetric line element (5). To this end, we consider the point-particle Lagrangian density given by

$$\mathcal{L} = \frac{1}{2}g_{\mu\nu}\dot{x}^\mu\dot{x}^\nu = \epsilon, \quad (7)$$

where \dot{x}^μ is the four-velocity of the photon, $\epsilon = (-1, 0, 1)$ indicates the time-like, null, or space-like character of the geodesic, respectively, and an overdot denotes the derivative with respect to the affine parameter λ . Taking into account the metric (5) yields the following form for

the Lagrangian

$$\mathcal{L} = \frac{1}{2} \left[-A(r)\dot{t}^2 + \frac{\dot{r}^2}{A(r)} + C(r)\dot{\theta}^2 + C(r)\sin^2\theta\dot{\phi}^2 \right] = \epsilon. \quad (8)$$

Given the spherically symmetric character of the space-time, we can consider the motion in the equatorial plane, $\theta = \pi/2$, without any loss of generality. In addition, since the Lagrangian (7) does not directly depend on t and ϕ , the Euler-Lagrange equations imply the conservation of two quantities:

$$E = A(r)\dot{t}, \quad (9a)$$

$$L = C(r)\dot{\phi}, \quad (9b)$$

where E is the energy of the particle and L the angular momentum, respectively (per unit mass). Since we are interested in null geodesics, $\epsilon = 0$, Eq. (7) with the conserved quantities (9a) and (9b), leads to

$$\dot{r}^2 = \frac{1}{b^2} - V_{\text{eff}}(r). \quad (10)$$

where we have conveniently re-absorbed a factor L in the affine parameter λ , and introduced the impact parameter $b \equiv L/E$. In this equation, the effective potential reads as

$$V_{\text{eff}}(r) = \frac{A(r)}{C(r)}. \quad (11)$$

which for the metric function considered in this work, Eq. (6), reads

$$V_{\text{eff}}(r) = \frac{1}{r^2} - \frac{2M}{r^3} + \frac{\gamma}{r}. \quad (12)$$

The maximum of the effective potential determines the region of unstable orbits, dubbed as the *photon sphere*, whose radius is denoted by $r = r_p$, and the corresponding impact parameter as the *critical impact parameter*, dubbed by b_c . The latter separates those orbits that are captured by the black hole, $b < b_c$, from those that are scattered back to asymptotic infinity, $b > b_c$. Those that have $b = b_c$ may linger indefinitely at the photon sphere, turning several times around the black hole. To determine these quantities, we note that circular light orbits obey $\dot{r} = 0$ and $\ddot{r} = 0$ simultaneously. Under these conditions, r_p and b_c are expressed for the metric function (6) as

$$r_p = \frac{\sqrt{1 + 6\gamma M} - 1}{\gamma}, \quad (13a)$$

$$b_c = \frac{3\sqrt{6}M}{\sqrt{(1 + \sqrt{1 + 6\gamma M} + 6\gamma M)\sqrt{1 + 6\gamma M} + 9\gamma M}}, \quad (13b)$$

which for $\gamma = 0$ it recovers the critical $b_c = 3\sqrt{3}M$ and the photon sphere radius $r_p = 3M$ of the Schwarzschild geometry.

With the expressions (9b) and (10) we can develop the equation of motion which describes the trajectory of the photon as

$$\left(\frac{dr}{d\phi}\right)^2 = C^2(r) \left(\frac{1}{b^2} - V_{\text{eff}}\right). \quad (14)$$

These are the general expressions for a given spherically symmetric metric.

B. Shadow's radius and constraints to the γ parameter

The shadow of a black hole is a silhouette, a region marked by a strong decrease in the observed luminosity, projected onto the celestial plane of a distant observer. This projection arises from photons originating from a background source, which are absorbed due to its intense gravity. To calculate the angular size and the shadow of the black hole, we adopt the formalism described by [50]. In this approach, they consider a static observer located at $(r_0, \theta_0 = \pi/2)$, projecting an angle θ relative to the radial coordinate r , as given by

$$\tan \theta = \sqrt{\frac{C(r)}{A^{-1}(r)} \frac{d\phi}{dr}} \Big|_{r=r_0}. \quad (15)$$

The shadow of the black hole, understood as the region which borders (on the observer's plane image) the critical curve, is thus constructed by the light rays emitted from the observer back to the source.

To proceed with our derivation, we conveniently rewrite Eq.(14) into

$$\left(\frac{dr}{d\phi}\right)^2 = \frac{C(r)}{A^{-1}(r)} \left(\frac{C(r)}{A(r)} \frac{E^2}{L^2} - 1\right). \quad (16)$$

A light ray with impact parameter $b > b_c$ will be scattered off the black hole at a radial distance $r_0 > r_m$, while the photon sphere (i.e. the locus of unstable bound geodesics, r_p) can be found via the condition $dr/d\phi|_{r_p} = 0$ which allows to express the impact parameter b as

$$\frac{1}{b^2} = \frac{A(r_p)}{C(r_p)}. \quad (17)$$

Now, by introducing the definition

$$h^2(r) = \frac{C(r)}{A(r)}, \quad (18)$$

we can rewrite Eq. (16) as

$$\left(\frac{dr}{d\phi}\right)^2 = \frac{C(r)}{A^{-1}(r)} \left(\frac{h^2(r)}{h^2(r_p)} - 1\right). \quad (19)$$

Substituting Eq.(19) into Eq.(15), and after proper manipulations, allows to find the expression

$$\sin^2 \theta = \frac{h^2(r_p)}{h^2(r_0)}, \quad (20)$$

which yields the angular size of the black hole's shadow θ_s as

$$\sin^2 \theta_s = \frac{b_c^2}{h^2(r_0)} = \frac{b_c^2 A(r_0)}{C(r_0)}. \quad (21)$$

Using the expressions worked out above, for CG the angular shadow's size reads as

$$\begin{aligned} \sin^2 \theta_s = & \frac{2}{r_0^2 \gamma^2 (\gamma + 8\gamma^2 M)} \left(-1 + 6M \sqrt{(1 + 6\gamma M)} \right. \\ & \left. + \sqrt{(1 + 6\gamma M) - 9\gamma M} \right) \left(1 - \frac{2M}{r_0} + \gamma r_0 \right) \end{aligned} \quad (22)$$

Similarly, we can obtain an expression for the shadow radius as seen by a far-away observer, a regime in which we approximate $\sin(\theta) \sim \theta$ and $\theta_s = b_c/r_0$ which gives us the following relation (assuming $\theta = \pi/2$)

$$r_s = r_p \sqrt{\frac{g_{tt}(r_0)}{g_{tt}(r_p)}}. \quad (23)$$

For CG this reads as

$$r_s = \frac{(\sqrt{a} - 1)}{\gamma} \sqrt{\frac{(\sqrt{a} - 1) [r_0 (\gamma r_0 + 1) - 2M]}{r_0 (1 - \sqrt{a} + 4\gamma M)}}, \quad (24)$$

where $a = 1 + 6\gamma M$. In Fig. 1 we depict the behaviour of the shadow's radius in CG with the parameter γ , considering the black hole distance and mass estimates reported in Table I.

We now aim to restrict the parameter space of γ by assessing the compatibility of the CG geometry's corresponding shadow radius r_s with the EHT's inferred shadow size of Sgr A* using the data above. This is so because, as argued in [52], it is reported that the observed shadow size of Sgr A* can be inferred by utilizing the size of the bright emission ring as its proxy, subject to a calibration factor that multiplicatively accounts for the theoretical and observational uncertainties. Such a correlation becomes possible thanks to priors on Sgr A*'s mass-to-distance ratio obtained via orbital dynamics measurements of the stars closest to the galactic center (i.e. dubbed S-stars), and which are reported in Table I. These measurements allow the EHT collaboration to estimate the fractional deviation δ between Sgr A*'s inferred shadow size r_{sh} and that of a Schwarzschild black hole $r_{sh,Sch} = 3\sqrt{3}M$, with angular radius $\omega_g = M/D$ via the formula

$$r_{sh}/M = (\delta + 1)3\sqrt{3}, \quad (25)$$

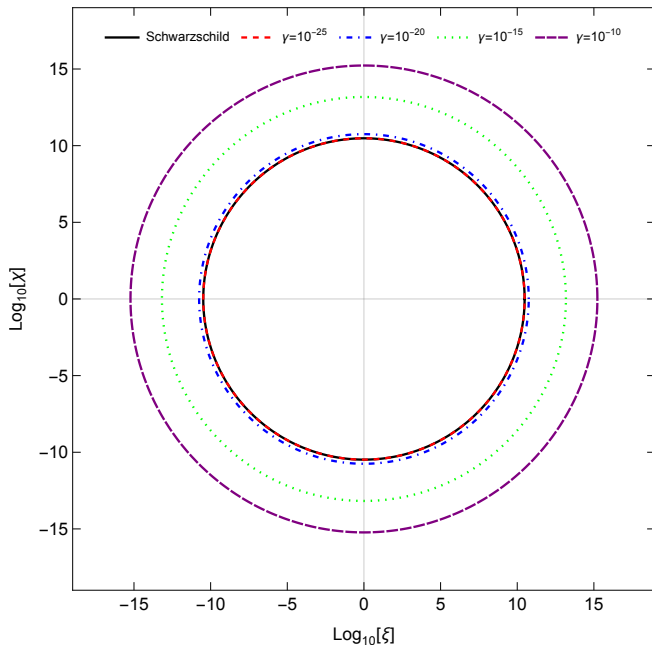


Figure 1: Shadow of a black hole in the plane in the celestial plane, expressing the celestial coordinates (ξ, χ) in a logarithmic scale, for the Schwarzschild geometry (black) and for CG with $\gamma = 10^{-25}, 10^{-20}, 10^{-15}$ and 10^{-10} (colored and dashed lines).

which, under the assumption of a normal distribution of the estimation uncertainties, yields the following shadow size bounds [43]

$$4.55 \lesssim r_{sh}/M \lesssim 5.22, \quad (26)$$

at 1σ deviation and

$$4.21 \lesssim r_{sh}/M \lesssim 5.56, \quad (27)$$

at 2σ deviation.

Parameter values			
Survey	$M (\times 10^6 M_\odot)$	D (kpc)	Reference
Keck	3.951 ± 0.047	$7.953 \pm 0.050 \pm 0.032$	[51]

Table I: Sgr A* Mass and distance.

We note that, to quantify the theoretical biases in the calibration factor utilized in the inference of the shadow's size of Sgr* A, the EHT collaboration performs simulations of black hole images to study a wide range of effects concerning the accretion flow properties and the underlying space-time. In this regard, the collaboration assumes the Kerr metric by default, although they also cover black hole metrics that either deviate from the Kerr space-time or describe alternative geometries, such as wormholes or boson stars. Because their analysis does not include the

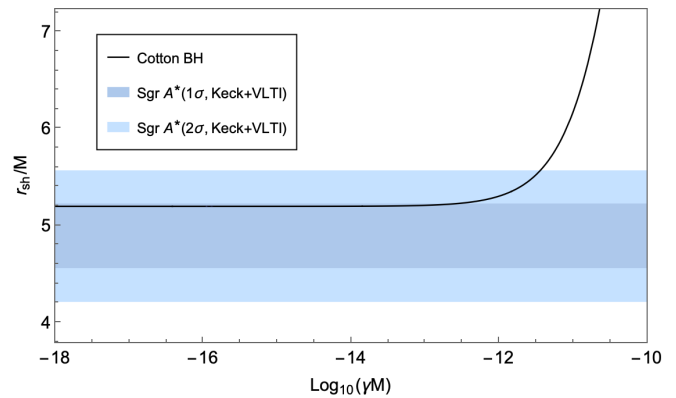


Figure 2: Shadow radius r_{sh} of a Cotton Gravity black hole (solid black curve) with a metric function provided by Eq.(6), as a function of the logarithm of γM , and calculated according to equation (24), for an observer located at $r_O \sim 8000$ kpc. The shaded blue and light blue regions represent the 1σ and 2σ EHT constraints, respectively, to the shadow radius of Sgr A*.

Cotton geometry, by performing tests with the above constraints we introduce a theoretical bias in our own analysis, since we assume these results to be valid for the CG spacetime. The extent to which the Cotton geometry could modify the above fractional deviation, and the constraints stemming from it, could be evaluated by performing a similar analysis to that by the EHT collaboration. However, such an effort lies well beyond the purpose of this work.

To perform tests on the CG metric with its shadow radius, we compare the evolution of r_s as a function of the logarithm of γM , in Fig. 2. We restrict our analysis to positive values of γ , which are required to describe the large-distance gravitational acceleration. Because we are dealing with a non-asymptotically flat space-time, one must take into account that its asymptotic Arnowitt-Deser-Misner (ADM) mass [53] is undefined for an observer at radial infinity and cannot be associated with the mass parameter appearing in the metric. To circumvent this issue, we shall take a similar approach to [43] and report the the shadow radius in units of the local mass M , based on the reasoning that the stellar orbital dynamics of the S group of stars probe this quantity, since they are influenced by the local gravity of Sgr A*. Additionally, since the CG black hole's shadow radius depends explicitly on the observer's radial position, recall Eq.(24), we compute the shadow radius considering an observer located at $r_O \sim 8000$ kpc [51].

Upon inspection of Fig. 2, we verify that r_{sh} starts to increase around values of $\gamma M \sim 10^{-12}$. Below this value, the CG black hole shadow radius coincides with that of a Schwarzschild black hole. We note that this is qualitatively the same behavior that is evidenced in [43] for the Rindler metric. Actually, the contribution of γ to the shadow radius becomes significant when the term $\gamma r \gg 1$, while the upper 2σ bound in Eq.(27) becomes satu-

rated at a value of approximately $\gamma M \simeq 3.525 \times 10^{-12}$. For the values of γM predicted by galaxy radial acceleration rotation curves in [13], or the recent constraints obtained by analyzing CG's influence on CMB power spectrum and large scale structures [54] (i.e. both estimating $\gamma M \sim 10^{-17}$), the shadow radius of the Cotton black hole lies well within the constraints imposed by Sgr A*'s shadow bounds, though there is no appreciable difference between it and its Schwarzschild counterpart. This result is not surprising, given that γ encodes large-distance gravitational effects within the CG framework. We have also found that the Cotton black hole shadow radius remains within the 2σ bounds for $\gamma M \sim 10^{20}$. Such values describe extremely large and unphysical gravitational acceleration effects, exceeding any other current estimates by several orders of magnitude. For this reason, we have opted for excluding them from the γ parameter range in Fig. 2.

IV. GRAVITATIONAL LENSING

This section deals with the phenomenon of gravitational lensing for CG. First, we will obtain the exact analytical expression for the deflection angle in terms of elliptic integrals. Then we will calculate an approximate expression valid for the weak field regime.

A. Exact deflection angle

To proceed with our derivation, it is convenient to make the following variable change in the radial coordinate $u = 1/r$ in Eq. (14). This allows us to re-write the photon equation of motion as

$$\left(\frac{du}{d\phi}\right)^2 = 2MG(u), \quad (28)$$

where the function $G(u)$ reads, for CG, as

$$G(u) = u^3 - \frac{u^2}{2M} - \frac{u\gamma}{2M} + \frac{1}{2Mb^2}. \quad (29)$$

The general expression for the deflection angle at a finite distance has been worked out in [55] as

$$\alpha = \sqrt{\frac{1}{2M}} \left(\int_{u_R}^{u_0} \frac{du}{\sqrt{G(u)}} + \int_{u_S}^{u_0} \frac{du}{\sqrt{G(u)}} \right) + \Psi_R - \Psi_S, \quad (30)$$

where $u_0 = 1/r_0$ is the inverse of the distance of closest approach, while $u_R = 1/r_R$ and u_S are the inverse of the radius of the observer and the source, respectively, and the indices refer to the position of the observer (R) and the source (S). The function Ψ encodes a correction term accounting for the finite distance, and is given by

$$\Psi = \arcsin \left(bu\sqrt{A(u)} \right). \quad (31)$$

Note that if we take the limit of $\gamma \rightarrow 0$, and consider also that observer and source are located at infinity we will have

$$\alpha_{SC} = \sqrt{\frac{2}{M}} \int_0^{u_0} \frac{du}{\sqrt{G(u)}} - \pi, \quad (32)$$

which is the well-known deflection angle formula for the Schwarzschild solution. This change in the definition of the deflection angle is necessary because the Cotton metric is not asymptotically flat. Moving on, the integrals of Eq. (30) can be solved by rewriting the function $G(u)$ as

$$G(u) = (u - u_1)(u - u_2)(u - u_3), \quad (33)$$

where u_1, u_2 and u_3 are the roots of the cubic polynomial. We can check that $u_0 = 1/r_0$ is one of the roots of this polynomial. We have chosen (for reasons that will become clear later) $u_2 = 1/r_0$. Now we can write

$$u^3 - u^2 \left(u_1 + u_3 + \frac{1}{r_0} \right) + u \left(u_1 u_3 + \frac{u_1}{r_0} + \frac{u_3}{r_0} \right) - u_1 \frac{u_3}{r_0} = u^3 - \frac{u^2}{2M} - \frac{u\gamma}{2M} + \frac{1}{2Mb^2}. \quad (34)$$

After comparing the coefficients in Eq. (34), we get

$$\begin{aligned} u_1 + u_3 + \frac{1}{r_0} &= \frac{1}{2M}, \\ u_1 u_3 + \frac{u_1}{r_0} + \frac{u_3}{r_0} &= -\frac{\gamma}{2M}. \end{aligned} \quad (35)$$

Solving the above system we find that u_1 and u_3 are given by

$$\begin{aligned} u_1 &= \frac{-2M + r_0 \mp \sqrt{-(12M^2 - 8\gamma M r_0^2 - 4M r_0 - r_0^2)}}{4M r_0}, \\ u_3 &= \frac{-2M + r_0 \pm \sqrt{-(12M^2 - 8\gamma M r_0^2 - 4M r_0 - r_0^2)}}{4M r_0}, \end{aligned} \quad (36)$$

respectively. Note that we have two different solutions, one of which is $u_1 > u_3$ and another that $u_3 > u_1$. Since our goal is that these roots fulfill the condition $u_3 > u_2 > u_1$, we choose the negative sign in the expression u_1 and the positive sign in the expression u_3 . Now both integrals of Eq. (30) can be put into the form

$$I_1(u') = \int_{u'}^{u_2} \frac{du}{\sqrt{(u - u_1)(u - u_2)(u - u_3)}} \quad (37)$$

with $u_3 > u_2 > u' > u_1$ and u' being any finite distance. The result of the above integral is

$$I(u') = \frac{2}{\sqrt{u_3 - u_1}} F(\delta, k^2), \quad (38)$$

where $F(\delta, k^2)$ is an incomplete first-order elliptic integral of the parameters

$$\delta = \arcsin \sqrt{\frac{(u_3 - u_1)(u_2 - u')}{(u_2 - u_1)(u_3 - u')}}}, \quad (39)$$

$$k^2 = \frac{u_2 - u_1}{u_3 - u_1}. \quad (40)$$

To get the result of the integrals given in (30) we just need to evaluate $I(u_R) + I(u_S)$. The complete result will also depend on the correction given by the functions $\Psi(u_R) - \Psi(u_S)$. For the Cotton metric, the function Ψ is

$$\Psi(u) = \sin^{-1} \left(bu \sqrt{1 - 2Mu + \frac{\gamma}{u}} \right), \quad (41)$$

while we have for the parameters

$$\delta(u') = \sin^{-1} \left\{ 2\sqrt{2} \left[\left(\frac{Mr_0(1 - u'r_0)\sqrt{r_0^2 c}}{\sqrt{r_0^2 c + 6Mr_0 - r_0^2}} \right) \times \left(\sqrt{r_0^2 c - 2Mr_0(2Rr_0 + 1) + r_0^2} \right)^{-1} \right]^{1/2} \right\}, \quad (42)$$

where $c = -12M^2 + 4Mr_0(2\gamma r_0 + 1) + r_0^2$

$$k^2 = \frac{\sqrt{r_0^2 - 12M^2 + 4Mr_0(2\gamma r_0 + 1) + 6M - r_0}}{2\sqrt{r_0^2 - 12M^2 + 4Mr_0(2\gamma r_0 + 1)}}. \quad (43)$$

which closes all the expressions we needed to characterize the deflection angle in CG. It is also interesting to re-write these expressions in terms of the impact parameter by inverting its definition, in CG, as

$$r_0 = \frac{b^2\gamma}{3} + \frac{2}{3}b\sqrt{b^2\gamma^2 + 3} \times \cos \left[\frac{1}{3} \cos^{-1} \left(\frac{(2b^4\gamma^3 + 9b^2\gamma - 54M)}{2b(b^2\gamma^2 + 3)^{3/2}} \right) \right] \quad (44)$$

For the sake of the graphical representation of the deflection angle we prefer to use the variable $b' = 1 - b_c/b$. This variable is limited to a value between $0 \leq b' \leq 1$, where zero represents the strong field limit and one the weak field one. In Figs. 3 and 4 we show the deflection angle as a function of the variable b' for values of γ in the range from 10^{-16} to 10^{-9} . We see that α decreases with increasing γ and that there is no significant change in the values of α from $\gamma < 10^{-13}$. If we increase the value of the parameter γ beyond the order of magnitude of 10^{-9} , the deflection angle begins to give negative values. Observationally, this value diverges for $b' = 0$ and tends to zero for $b' = 1$. We expect our theoretical result to reproduce this behaviour. In other words, for the phenomenon of light deflection, Cotton's parameter is limited to values smaller than $\gamma = 10^{-9}$.

V. IMAGES OF BLACK HOLES WITH THIN ACCRETION DISKS

Having restricted the γ -space parameter, we now proceed to generate the images of the Cotton black hole (by pushing the value saturating the upper 2σ bound of the Sgr A* shadow) and qualitatively compare its appearance to that of a Schwarzschild black hole of the same mass

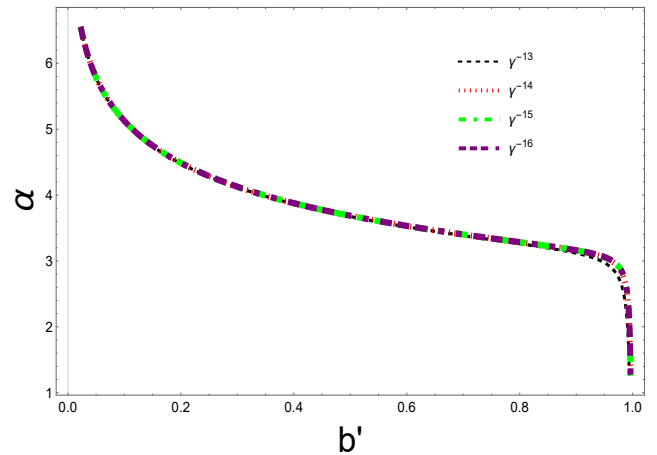


Figure 3: Graphical representation of the deflection angle α as a function of the reduced impact parameter b' for values of the CG parameter $\gamma = \{10^{-16}, 10^{-15}, 10^{-14}, 10^{-13}\}$.

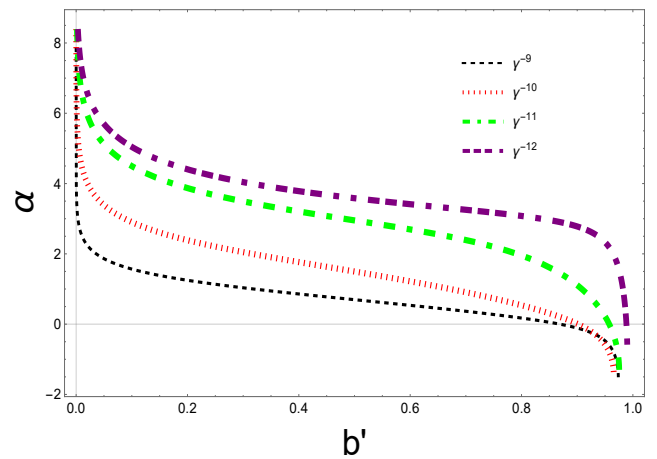


Figure 4: Graphical representation of the deflection angle α as a function of the reduced impact parameter b' for values of the CG parameter $\gamma = \{10^{-12}, 10^{-11}, 10^{-10}, 10^{-9}\}$.

parameter. We consider the setting of a black hole illuminated by an optically (i.e. fully transparent to its own radiation) and geometrically thin accretion disk, when observed at both a face-on inclination (i.e. $\theta_o = 0^\circ$) and at a nearly edge-on inclination (i.e. $\theta_o = 80^\circ$).

We begin our considerations from Eq. (14), which we conveniently re-write in the form

$$\frac{d\phi}{dr} = \pm \frac{b}{C(r)} \sqrt{\frac{1}{1 - b^2 V_{\text{eff}}}}, \quad (45)$$

that describes the variation in a photon's azimuthal angle as a function of its radial coordinate. By numerically ray-tracing the previous equation for a bunch of trajectories within some range of the impact parameter b , we compute the null geodesics from an observer's screen backwards towards their point of origin. Figure 5 displays the

geodesics in the Schwarzschild space-time (left panel) for $M = 1$, and in the CG space-time (right panel), the latter with a value of $\gamma M = 3.525 \times 10^{-12}$. Upon close observation of the figure, one highlights the absence of any significant qualitative differences between the near-horizon lensing properties of the two geometries, under the considered parameter values. In addition to larger distances, the effects of γ become more noticeable at much higher orders of magnitude than those considered here, as is discussed in Section IV below.

To simulate the emission from an accretion disk we resort to the semi-analytic models provided by Gralla, Lupsasca and Marrone in Ref. [44], which describe the radial emission profile of an accretion disk based on a Standard Unbound (SU) Johnson distribution function given by

$$I(r; \gamma, \mu, \sigma) = \frac{e^{-\frac{1}{2}[\gamma + \operatorname{arcsinh}(\frac{r-\mu}{\sigma})]^2}}{\sqrt{(r-\mu)^2 + \sigma^2}}, \quad (46)$$

where the γ, μ and σ parameters modify the skewness, peak location and kurtosis of the distribution, respectively. Such models are designed to reproduce the most prominent image features of time-averaged General Relativistic Magneto-Hydrodynamic (GRMHD) simulations of a thick accretion flow around a Kerr black hole, providing a less computationally taxing alternative towards the generation of black hole images [44]. These models describe an infinitesimally thin, axisymmetric, radially dependent emission profile, assumed to be monochromatic in the disk's frame of reference and optically thin at the emitting frequency. In the absence of absorption, the relativistic radiative transfer equation [56] implies that the specific intensity I_ν/ν^3 is conserved along a light ray such that $I_{\nu_o} = g^3 I_{\nu_e}$, where the subscripts o and e denote the observer and emitter frames, respectively. The quantity g is defined as the redshift factor $g = \nu_o/\nu_e = \sqrt{A(r)/A(r_\infty)}$. Since the disk is geometrically thin, a light ray gains additional brightness for each time it intersects the accretion disk while on its way to a distant observer (i.e. every n half-orbit). Thus, considering a monochromatic emitter $I_{\nu_e} \equiv I(r)$, the integrated (bolometric) intensity $I = \int I_{\nu_o} d\nu_o$ in the observer's plane is computed according to

$$I_o(r) = \sum_n \left(\frac{A(r)}{A(r_o)} \right)^2 I(r)|_{r=r_n}. \quad (47)$$

For the purpose of generating black hole images we restrict our analysis up to the $n = 2$ photon ring, as higher-order photon rings will provide a negligible contribution to the net luminosity (as shall be explained in the next section). We shall suitably adapt the three models introduced in [44] to a spherically symmetric scenario, to simulate the accretion flow around the Schwarzschild

and Cotton black holes, with the parameters

$$\text{GLM1} : \gamma = -\frac{3}{2}, \quad \mu = 0, \quad \sigma = \frac{M}{2}, \quad (48)$$

$$\text{GLM2} : \gamma = 0, \quad \mu = 0, \quad \sigma = \frac{M}{2}, \quad (49)$$

$$\text{GLM3} : \gamma = -2, \quad \mu = \frac{17M}{3}, \quad \sigma = \frac{M}{4}. \quad (50)$$

whose corresponding emission profile is depicted in Fig. 6.

The GLM1 and GLM2 models are utilized to simulate an accretion disk with an emission profile extending all the way towards the event horizon, being distinguished by the radial emission decay near this region. In contrast, the GLM3 model represents an accretion disk with its emission peak located near the radius of the innermost stable circular orbits (r_{ISCO}), which is $6M$ for a Schwarzschild black hole. The latter allows us to separate the individual luminosity contributions of the $n = 1$ and $n = 2$ rings from the direct emission, thereby facilitating the comparison of these features between the Schwarzschild and Cotton black holes, whereas in the former models the photon rings appear as a discrete set of boosts of luminosity superimposed on top of the disk's direct emission [40]. In our simulations, the observed luminosity is normalized with respect to its total value, to ensure both geometries are compared in identical settings. We resort to the Geodesic Rays and Visualization of IntensiTY profiles (GRAVITYp) ray-tracing code, developed by some of us.

By inspection of Fig. 7, we report no appreciable visual differences between a Schwarzschild and a Cotton black hole of the same mass, with $\gamma M \simeq 3.525 \times 10^{-12}$, regardless of the emission conditions. At the considered distance, the Cotton black hole's corresponding event horizon radius, photon sphere radius and critical impact parameter, are nearly indistinguishable from those of a Schwarzschild black hole of the same mass M , differing only by a factor of the same order of magnitude of γ . Since for a non-asymptotically flat geometry the shadow radius does not coincide with the critical impact parameter, the geometries appear identical. This similarity persists onto the photon ring(s), where the gravitational lensing features play a significant role. In the literature, however, various black holes with a similar critical impact parameter have been found to be distinguished by the properties of their corresponding photon rings [57]. These differences occur when, within the parameter space compatibility with Sgr A* shadow radius, the additional parameter in a given geometry modifies significantly the effective potential (i.e. its shape, location, concavity) seen by photons on their approach to a black hole, from the canonical Schwarzschild case. For some geometries, however, the constraints to the parameter space are too restrictive, to the point that there are virtually no changes to the effective potential, which is our case. Finally, we point out that although Eq. (47) suggests the observed intensity depends on the observer's

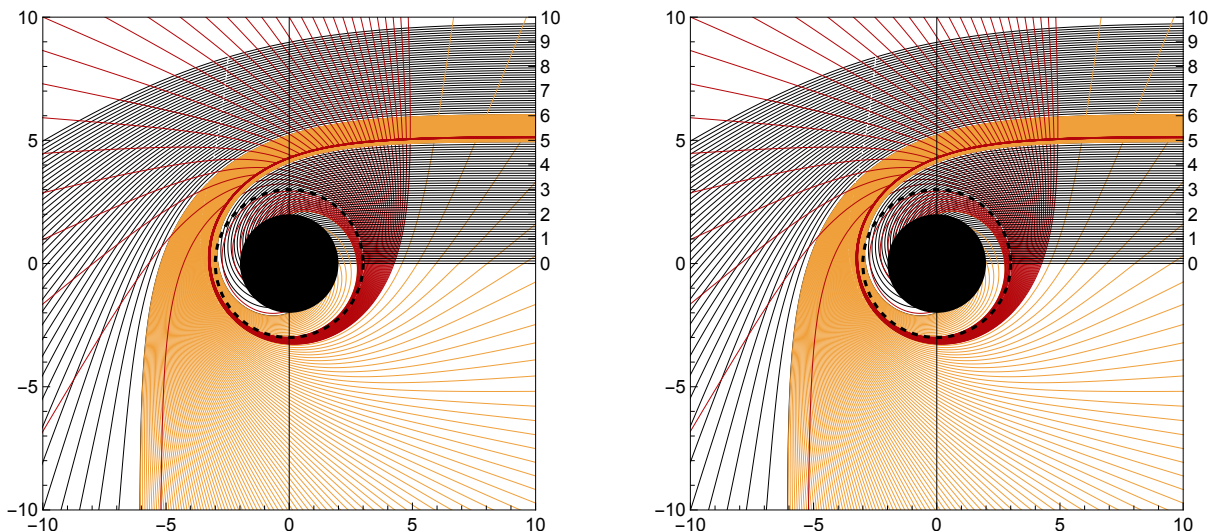


Figure 5: Null geodesics in the Schwarzschild space-time (left panel) and in the CG space-time as a function of impact parameter b normalized with respect to the mass parameter M . The photon trajectories are categorized according to the number of half-turns n around the black hole as the ($n = 0$) direct image (black), the $n = 1$ photon ring (gold), and the $n = 2$ photon ring (red), and with an impact parameter spacing of $1/5$, $1/50$, and $1/500$, respectively. The black circle depicts the inner region to the event horizon. The dashed black circumference represents the photon sphere radius. The black hole equatorial plane is represented by the black vertical line. The observer's screen is located on the right-side axis.

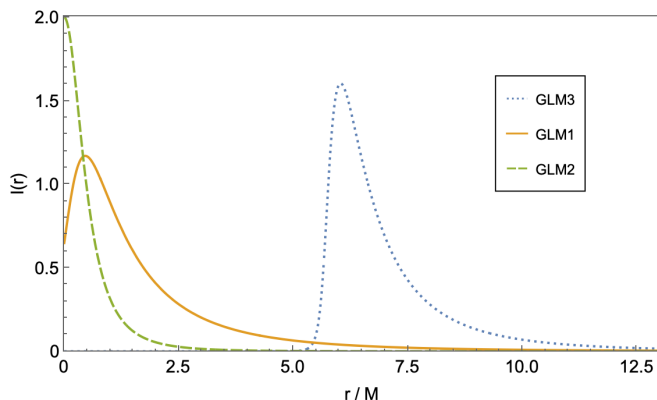


Figure 6: Emission profiles corresponding to the GLM1, GLM2 and GLM3 models described by the choice of parameters in Eqs. (48), (49) and (50), respectively, of the intensity function (46).

radial coordinate, for a non-asymptotically flat space-time, there are no visual differences between the Cotton and Schwarzschild black holes since the intensities are normalized with respect to their total value. Without normalizing the intensities, the observed intensities of the accretion disk emission in the Cotton spacetime would decrease, as in this case $A(r) \rightarrow \infty$ for an observer at infinity.

VI. ISORADIALS

In this section, we perform an analysis of isoradial curves in the Cotton and Schwarzschild space-times, to complement the black hole images presented in the previous section. We solve the isoradial equatorial curves corresponding to the $n = 0$ emission, following the analytical approximation provided by [58], which states that the arrival point of a light ray may be mapped onto an observer's plane with Cartesian coordinates (X', Y') as

$$\begin{bmatrix} X' \\ Y' \end{bmatrix} = \frac{R}{\sqrt{A(R)}} \sqrt{1 - (1-x)^2} \begin{bmatrix} \cos(\varphi) \\ \sin(\varphi) \end{bmatrix} \quad (51)$$

Here, R denotes a given radial distance from the origin, while φ corresponds to the polar angle in the observer's plane¹. The value of x may be computed via the following approximation

$$\begin{aligned} x = A(R)y & \left\{ 1 - \frac{e}{100} (1 - A(R))y \left[\ln \left(1 - \frac{y}{2} \right) + \frac{y}{2} \right] \right. \\ & + \frac{(315I_1^2 - 135I_2 + 180A^2(R) + 120I_1 + 32)}{720} y^2 \\ & \left. + \left(\frac{I_1}{2} + \frac{1}{6} \right) y \right\}, \quad (52) \end{aligned}$$

¹ For a better understanding of this coordinate representation, the reader is referred to Fig. 7 of [58].

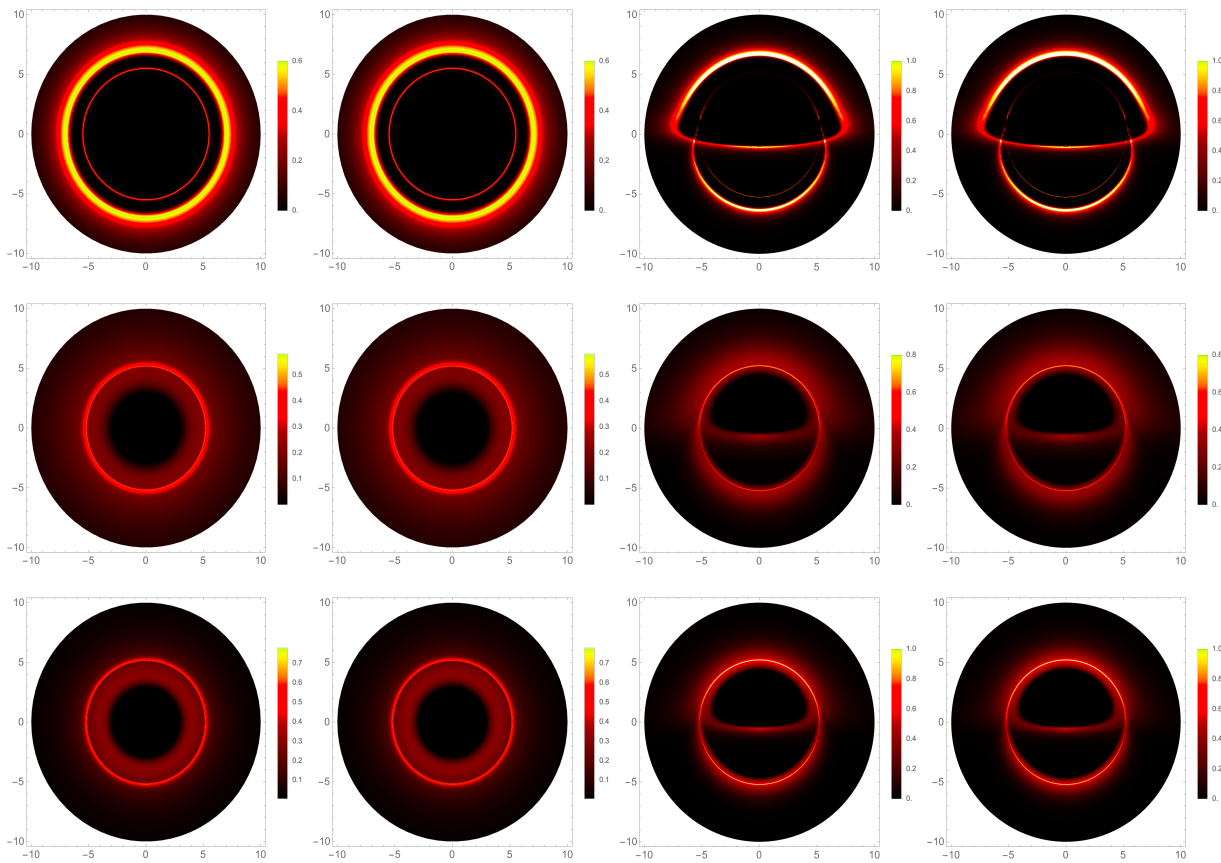


Figure 7: Visual appearance, in the impact parameter space, of the Schwarzschild black hole (1st and 3rd columns) and the CG black hole (2nd and 4th columns), for the GLM3 (top), GLM1 (middle) and GLM2 (bottom) emission profiles, for an observer located at a distance of $r_o = 1000M$, seen from a face-on orientation and from an inclination of 80° , respectively.

with y being expressed by the trigonometric relation between the polar angle in the observer's plane and the observer's inclination angle θ_o via

$$y = 1 + \frac{\sin(\varphi)}{\sqrt{\sin^2(\varphi) + \cot^2(\theta_o)}}, \quad (53)$$

and where the quantities I_1 and I_2 are calculated as

$$I_1 = \int_0^1 P(u) du, \quad I_2 = \int_0^1 P^2(u) du, \quad (54)$$

with $P(u) = -4u^2 A(u) + A(R)$, and where the variable change $r = R/u$ was considered to obtain $A(u)$.

By solving the above equations for all polar angles, for a light ray with its emission point located at a constant $r = R$, one obtains the isoradial curves of the $n = 0$ emission. In Fig. 8, we display isoradial curves for a Schwarzschild black hole and for a Cotton black hole with $\gamma M \simeq 3.525 \times 10^{-12}$, as seen by an observer with inclination angle $\theta_o = 80^\circ$.

This result emphasizes the similarity in the horizon-scale lensing phenomena between these two geometries, as seen by the complete overlap of the isoradial curve of

both space-times; something which is in agreement with the analysis in the previous section.

VII. THEORETICAL LYAPUNOV EXPONENT

In this section, we explore the Lyapunov exponent of nearly bound orbits, a quantity that measures the instability scale of such orbits. Since these instabilities take place near the photon sphere, the Lyapunov exponent tracks a local effect and is therefore independent of the observer's distance to the black hole. We begin our analysis by considering the effect of a small radial perturbation near the photon sphere (i.e. $r = \delta r + r_p$, $\delta r \ll r_p$) and apply it to Eq. (14). We perform a second-order Taylor series expansion of the effective potential V_{eff} around r_p

$$V_{\text{eff}}(r) \simeq V_{\text{eff}}(r_p) + V'_{\text{eff}}(r_p)\delta r + \frac{1}{2}V''_{\text{eff}}(r_p)(\delta r)^2, \quad (55)$$

where the first term of the expansion corresponds to the critical impact parameter b_c and the second term disappears, since unstable circular null geodesics correspond to critical maxima of the effective potential. The prime

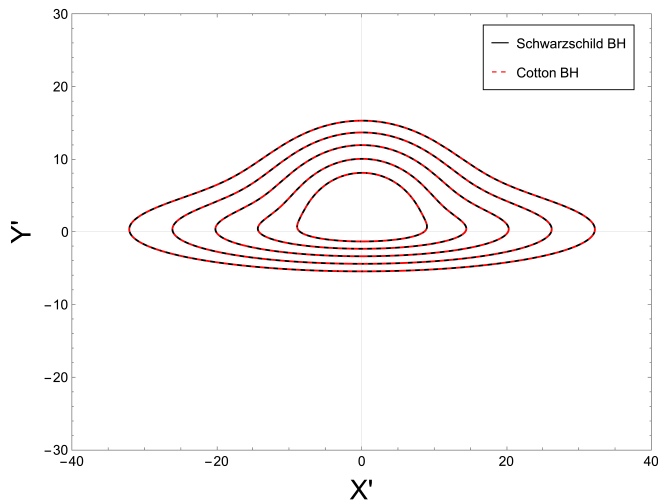


Figure 8: Isoradial curves at $R = 6M, 12M, 18M, 24M, 30M$ of a Schwarzschild black hole (black line) and a CG black hole with $\gamma M = 3.525 \times 10^{-12}$ (red dashed line), as seen by a distant observer with an observation angle $\theta_o = 80^\circ$.

notation above denotes a derivative with respect to the radial coordinate. Substituting this result into Eq. (14), leads to the following expression

$$\left(\frac{d\delta r}{d\phi}\right)^2 = -\frac{1}{2}C^2(r_p)V''_{\text{eff}}(r_p)(\delta r)^2. \quad (56)$$

By writing the differential equation in the form

$$\pi \frac{d\delta r}{d\phi} = \lambda \delta r, \quad (57)$$

whose solutions are of an exponential form, $\delta r_n = \delta r_0 e^{\lambda n}$, we obtain the Lyapunov exponent λ which quantifies the instability scale of a small perturbation. Computing the second derivative of the effective potential and utilizing the critical curve equation $C'(r_p)A(r_p) - C(r_p)A'(r_p) = 0$ [59], yields the following expression for the theoretical Lyapunov exponent

$$\lambda = \pi \left(\frac{AC'' - A''C}{2} \right)^{\frac{1}{2}}. \quad (58)$$

For the Schwarzschild geometry $\gamma = \pi$, indicating that an initial perturbation grows (in radial distance) by a factor e^γ with each half-orbit around the black hole. For the Cotton geometry, the Lyapunov exponent reads

$$\lambda = \pi(1 + \gamma r_p)^{\frac{1}{2}}. \quad (59)$$

This result supports the qualitative analysis done in the previous sections. The λ exponent of the CG black hole, differs from the Schwarzschild black hole by an order of magnitude proportional to γ . Consequently, despite the exponential behaviour driven by the Lyapunov exponent, the deviations between these two geometries are

captured by photon rings of a similarly order, requiring many half-orbits around the black hole before becoming significantly different. The gravitational lensing causing the $n = 1$ and $n = 2$ photon rings is far from being sensitive to the contribution of γ . Thus, one cannot hope to be able to distinguish between the Schwarzschild and CG geometries via their $n = 1$ and $n = 2$ ring features (i.e. relative intensities, relative widths), which are the ones that could be within reach of future interferometric detectors [60].

VIII. CONCLUSION

In this work we investigate the phenomenon of gravitational lensing and its associated observables within an extension of GR recently proposed in the literature and dubbed as Cotton gravity. We estimated the size of the new parameter γ of Cotton gravity and which arises with a newly found spherically symmetric vacuum (Schwarzschild-like) solution, by making a numerical comparison with bound on the shadow's size of the supermassive black hole at the center of our galaxy (Sgr A*) reported by the Event Horizon Telescope Collaboration. Such a bound is saturated, for CG, for values as small as $\gamma M = 3.525 \times 10^{-12}$ (at 2σ in such bounds), where we took into account some subtleties associated to the non-asymptotic flatness of CG geometry to identifying the mass parameter of it with the one of the Schwarzschild case.

To study the impact of this result in geodesic effects, we first computed the exact expression for the deflection angle in the form of elliptic integrals. There are two important considerations about this result. Firstly, in order to obtain the result of the Schwarzschild solution, one must first assume $\gamma = 0$ and additionally u_R and $u_S = 0$ (which corresponds to the consideration of infinite distances). This is because the result for Schwarzschild is usually determined using the definition for infinite distances, which is not possible in the case of Cotton gravity given its non-asymptotically flat character. Secondly, the deflection angle can be written as a function of the impact parameter b , though under an explicit cumbersome form. Furthermore, we computed the deflection angle using a Taylor series approximation to solve the integrals, which yields a result which is valid for the weak field regime where $M/b \ll 1$. We have considered a linear approximation for the parameter γ in addition to the series with respect to the mass (we expect that γ has in reality a much smaller order of magnitude than mass and distances), and checked the consistence of the analytical approximation with the numerical integration of the deflection angle. Overall, we find that the deflection angle remains unchanged for values of the CG parameter $\gamma < 10^{-14}$.

The smallness of such a parameter of CG drove us to consider the chances of distinguishing between Schwarzschild and CG black holes using observables asso-

ciated to gravitational lensing. To this end, we simulated the appearance of a CG black hole, with such a value of the γ parameter, surrounded by a thin accretion disk, modelled by three semi-analytic radial intensity profiles. We found the constraints placed on γ by Sgr A*'s shadow bounds to be too tight for any significant visual differences to appear. In this regard, we note that although in CG the observed intensity depends on the observer's radial distance, our images do not show any difference in this regard due to having normalized intensity profiles.

In looking for further settings to search for the presence of any differences, we studied the isoradial curves of a CG black hole against those of a Schwarzschild black hole, utilizing a generalization of the Poutanen formula. We found that there is a full overlap of the isoradial curves between the CG and Schwarzschild geometries, confirming the absence of any visual differences in this regard. We also considered the theoretical Lyapunov exponent for a Cotton gravity black hole, associated to the instability scale of photon rings. We derived its exact expression by perturbing the photon equation of motion about the photon sphere radius. The CG theoretical Lyapunov exponent was found to differ from Schwarzschild's by a factor proportional to CG's γ parameter, and thus photon rings do not help in discriminating between both geometries, at least for those rings ($n = 1$ and $n = 2$) that could be expected to be measured in the last decades via interferometric means.

To conclude, the analysis carried out in this work points that the CG space-time recently found in the literature is very unlikely to be distinguishable from the expectations of the canonical Schwarzschild black holes with the devices we have at this moment and in the foreseeable near future.

ACKNOWLEDGMENTS

MER thanks Conselho Nacional de Desenvolvimento Científico e Tecnológico - CNPq, Brazil, for partial financial support. This study was financed in part by the Coordenação de Aperfeiçoamento de Pessoal de Nível Superior - Brasil (CAPES) - Finance Code 001. FSNL acknowledges support from the Fundação para a Ciência e a Tecnologia (FCT) Scientific Employment Stimulus contract with reference CEECINST/00032/2018, and funding through the research grants UIDB/04434/2020, UIDP/04434/2020 and PTDC/FIS-AST/0054/2021. DRG is supported by the Spanish Agencia Estatal de Investigación Grant No. PID2022-138607NB-I00, funded by MCIN/AEI/10.13039/501100011033, UE (European Union), ERDF (European Regional Development Fund) A way of making Europe.

-
- [1] C. M. Will, *Living Rev. Rel.* **17** (2014) 4.
 - [2] A. G. Riess *et al.* [Supernova Search Team], *Astron. J.* **116** (1998) 1009.
 - [3] S. Perlmutter *et al.* [Supernova Cosmology Project], *Astrophys. J.* **517** (1999) 565.
 - [4] E. J. Copeland, M. Sami and S. Tsujikawa, *Int. J. Mod. Phys. D* **15**, 1753-1936 (2006).
 - [5] S. M. Carroll, *Living Rev. Rel.* **4** (2001), 1.
 - [6] J. M. M. Senovilla, *Gen. Rel. Grav.* **54** (2022) 151.
 - [7] P. Salucci, A. Lapi, C. Tonini, G. Gentile, I. Yegorova and U. Klein, *Mon. Not. Roy. Astron. Soc.* **378** (2007), 41-47.
 - [8] S. W. Hawking, *Phys. Rev. D* **72** (2005) 084013.
 - [9] C. Rovelli, "Quantum Gravity", Cambridge University Press (Cambridge Monographs on Mathematical Physics, 2004.).
 - [10] T. Clifton, P. G. Ferreira, A. Padilla and C. Skordis, *Phys. Rept.* **513** (2012) 1.
 - [11] S. Capozziello and M. De Laurentis, *Phys. Rept.* **509** (2011) 167.
 - [12] J. Harada, *Phys. Rev. D* **103** (2021) L121502.
 - [13] J. Harada, *Phys. Rev. D* **106** (2022) 064044.
 - [14] S. Capozziello, V. F. Cardone, S. Carloni and A. Troisi, *Phys. Lett. A* **326** (2004), 292-296.
 - [15] S. Capozziello, V. F. Cardone and A. Troisi, *Mon. Not. Roy. Astron. Soc.* **375** (2007), 1423-1440.
 - [16] C. G. Boehmer, T. Harko and F. S. N. Lobo, *Astropart. Phys.* **29** (2008), 386-392.
 - [17] C. G. Boehmer, T. Harko and F. S. N. Lobo, *JCAP* **03** (2008), 024.
 - [18] S. Capozziello, T. Harko, T. S. Koivisto, F. S. N. Lobo and G. J. Olmo, *JCAP* **07** (2013), 024.
 - [19] S. Capozziello, T. Harko, T. S. Koivisto, F. S. N. Lobo and G. J. Olmo, *Astropart. Phys.* **50-52** (2013), 65-75.
 - [20] R. A. Sussman and S. Najera, [[arXiv:2312.02115](#)] [gr-qc].
 - [21] M. Gogberashvili and A. Girgvliani, *Class. Quant. Grav.* **41** no.2, 025010 (2024).
 - [22] C. A. Mantica and L. G. Molinari, *Gen. Rel. Grav.* **55** (2023) no.4, 62
 - [23] R. A. Sussman and S. Najera, [[arXiv:2311.06744](#)] [gr-qc].
 - [24] G. Clément and K. Nouicer, [[arXiv:2312.17662](#)] [gr-qc].
 - [25] R. A. Sussman, C. A. Mantica, L. G. Molinari and S. Nájera, [[arXiv:2401.10479](#)] [gr-qc].
 - [26] G. Clément and K. Nouicer, [[arXiv:2401.16008](#)] [gr-qc].
 - [27] R. A. Sussman, C. A. Mantica, L. G. Molinari and S. Nájera, [[arXiv:2402.01992](#)] [gr-qc].
 - [28] Arthur B. Congdon, and Charles R. Keeton, "Principles of Gravitational Lensing: Light Deflection as a Probe of Astrophysics and Cosmology", Springer, (2018).
 - [29] V. Bozza, *Phys. Rev. D* **66** (2002) 103001.
 - [30] V. Bozza and L. Mancini, *Astrophys. J.* **753** (2012) 56.
 - [31] S. Pietroni and V. Bozza, *JCAP* **12** (2022),j 018.
 - [32] N. Tsukamoto, *Phys. Rev. D* **102** (2020) 104029.
 - [33] N. Tsukamoto, *Phys. Rev. D* **103** (2021) 024033.
 - [34] N. Tsukamoto, *Phys. Rev. D* **104** (2021) 124016.
 - [35] J. Zhang and Y. Xie, *Eur. Phys. J. C* **82** (2022) 471.

- [36] S. E. Gralla, D. E. Holz and R. M. Wald, *Phys. Rev. D* **100** (2019) 024018.
- [37] H. Falcke, F. Melia and E. Agol, *Astrophys. J. Lett.* **528** (2000) L13.
- [38] P. V. P. Cunha and C. A. R. Herdeiro, *Gen. Rel. Grav.* **50** (2018) 42.
- [39] S. E. Gralla and A. Lupsasca, *Phys. Rev. D* **101** (2020) 044031.
- [40] M. D. Johnson, *et al. Sci. Adv.* **6** (2020) eaaz1310.
- [41] K. Akiyama *et al.* [Event Horizon Telescope], *Astrophys. J. Lett.* **875** (2019) L1.
- [42] K. Akiyama *et al.* [Event Horizon Telescope], *Astrophys. J. Lett.* **930** (2022) 12.
- [43] S. Vagnozzi, *et al. Class. Quant. Grav.* **40** (2023) 165007.
- [44] S. E. Gralla, A. Lupsasca and D. P. Marrone, *Phys. Rev. D* **102** (2020) 124004.
- [45] P. D. Mannheim and D. Kazanas, *Astrophys. J.* **342** (1989) 635.
- [46] S. G. Ghosh, L. Tannukij and P. Wongjun, *Eur. Phys. J. C* **76** (2016) 119.
- [47] S. Soroushfar, R. Saffari, J. Kunz and C. Lämmerzahl, *Phys. Rev. D* **92** (2015) 044010.
- [48] V. V. Kiselev, *Class. Quant. Grav.* **20** (2003) 1198.
- [49] D. Grumiller, *Phys. Rev. Lett.* **105** (2010), 211303 [erratum: *Phys. Rev. Lett.* **106** (2011)].
- [50] V. Perlick and O. Y. Tsupko, *Phys. Rept.* **947** (2022) 1.
- [51] T. Do, *et al. Science* **365** (2019) 664.
- [52] K. Akiyama *et al.* [Event Horizon Telescope], *Astrophys. J. Lett.* **930** (2022) L17.
- [53] R. L. Arnowitt, S. Deser and C. W. Misner, *Gen. Rel. Grav.* **40** (2008) 1997.
- [54] P. Xia, D. Zhang, X. Ren, B. Wang and Y. C. Ong, [[arXiv:2405.07209](https://arxiv.org/abs/2405.07209)] [astro-ph.CO].
- [55] A. Ishihara, Y. Suzuki, T. Ono, T. Kitamura and H. Asada, *Phys. Rev. D* **94** (2016) 084015.
- [56] R. Gold, *et al. Astrophys. J.* **897** (2020) 148.
- [57] L. F. D. da Silva, F. S. N. Lobo, G. J. Olmo and D. Rubiera-Garcia, *Phys. Rev. D* **108** (2023) 084055.
- [58] J. Claros and E. Gallo, [[arXiv:2403.18543](https://arxiv.org/abs/2403.18543)] [gr-qc].
- [59] C. M. Claudel, K. S. Virbhadra and G. F. R. Ellis, *J. Math. Phys.* **42** (2001) 818.
- [60] D. Ayzenberg, *et al.* [[arXiv:2312.02130](https://arxiv.org/abs/2312.02130)] [astro-ph.HE].